Journal of Alloys and Compounds 786 (2019) 1021–1029

Contents lists available at ScienceDirect

Journal of Alloys and Compounds

journal homepage: http://www.elsevier.com/locate/jalcom

Development of custom made bimetallic alloy model systems based on platinum – rhodium for heterogeneous catalysis

Susmit Kumar [a, *], David Waller [b], Helmer Fjellvåg [a, **], Anja Olafsen Sjåstad [a]

[a] Centre for Materials Science and Nanotechnology, University of Oslo, NO-0315, Oslo, Norway
[b] Yara Norge AS - Yara Technology Centre, NO-3905, Porsgrunn, Norway

ARTICLE INFO

Article history:
Received 11 September 2018
Received in revised form
15 January 2019
Accepted 3 February 2019
Available online 5 February 2019

Keywords:
Solid state diffusion
Platinum
Rhodium
Bimetallic alloys
Kirkendall effect

ABSTRACT

The current study extends the insight into solid-state diffusion in alloys of the Platinum Group Metals (PGMs). Thereby, we pave the way for tailor making surface compositions of binary platinum (Pt) – rhodium (Rh) model catalysts, with deposited rhodium layers on the surface of Pt single crystals (SCs) as the starting point. Platinum single crystals with (100), (110) and (111) orientations were studied by scanning electron microscopy (SEM) and energy dispersive X – ray spectroscopy (EDS). In addition, X – ray Photoelectron spectroscopy (XPS) characterization was carried out on Pt(110). The crystallographic orientation has a prominent effect on diffusion characteristics. The slowest moving Kirkendall – plane was observed for Pt(110) at $x_K = 250\,nm$ from reference point x_0, while, the fastest for Pt(100) was at $x_K = 450\,nm$, indicating that the inter-diffusion rate with respect to orientation increases in the sequence Pt(110) < Pt(111) < Pt(100). The diffusion coefficient of Rh into Pt is of the order $\sim 10^{-17}–10^{-18}\,m^2/s$, whereas it was slightly less than $\sim 10^{-19}\,m^2/s$ for Pt into Rh; albeit comparable to the vacancy diffusion rate from Pt into Rh. Our experimental findings show good agreement with calculated inter-diffusion coefficients using Darken analysis. A theoretical direction is proposed for improved fitting of data.

1. Introduction

Platinum group metals (PGMs) and their alloys find extensive industrial use. High temperature applications of platinum and/or platinum-rhodium binary alloys include B, R and S – type thermocouples; high temperature crucibles and heterogeneous catalysts for oxidation processes. In the case of the latter, there is a continuous and strong desire for optimizing PGM catalysts with respect to conversion and selectivity. Certain processes, such as ammonia oxidation (Ostwald process) and hydrogen cyanide production from methane and ammonia (Andrussow process), are highly exothermic, which, in turn affects the PGM composition via inter-diffusion, segregation and evaporation. In this respect, understanding of solid-state diffusion processes in well-defined model systems is needed, yet currently lacking. Recent works using Atom Probe Tomography (APT) on platinum (Pt) – rhodium (Rh) and Pt – Rh – palladium (Pd) alloys exposed to oxidizing and reducing environments reported nanoscale changes of relevance for design and production of nano-engineered catalysts [1,2]. Engineering of custom-made Pt – Rh alloy nanoparticles was reported recently by Kalyva et al. with potential specialized applications [3]. However, many industrial catalysts are currently, and will in the near future, be based on bulk materials, such as nets or gauzes, rather than on nanoparticles.

The literature on diffusion studies of PGMs (platinum group metals) is limited; however, some earlier works provide a good basis for the current study [4–9]. One new approach towards fundamental understanding into catalytic reaction mechanisms is to tailor the surface composition of well – defined model catalysts that are subsequently examined by a range of sensitive analytical tools. In the current investigation we address how inter-diffusion of deposited rhodium layers on platinum single crystals can provide solid solutions with compositional gradients extending from the external crystal surface and inwards. For this approach, an appropriate choice of temperature and anneal time is critical.

The analysis of the inter-diffusion of rhodium layers on Pt crystals, according to the open planar thin-film approach, is challenging. The theoretical foundation can be treated at various levels; simple diffusion of Rh into Pt according to the open planar film method; Rh into Pt and Pt into Rh interdiffusion, *i.e.*, the Kirkendall

* Corresponding author.
** Corresponding author.
E-mail addresses: susmit.kumar@kjemi.uio.no (S. Kumar), helmer.fjellvag@kjemi.uio.no (H. Fjellvåg).

https://doi.org/10.1016/j.jallcom.2019.02.026
0925-8388/

effect, combined with so − called Darken analysis to obtain the diffusion coefficient. Finally, the most complex but also the most realistic level, is to describe Rh into Pt and Pt into Rh inter-diffusion where the effects of compositional variations (chemical potential) are included in the diffusion coefficient. The experimental analysis is in itself challenging, whether based on x − ray photoelectron spectroscopy (XPS) with sputtering, dynamic secondary ion mass spectrometry (SIMS), or scanning electron microscopy (SEM)/energy dispersive x − ray spectroscopy (EDS) of cross-sections (or SIMS line − scans).

The experimental significance of a Kirkendall plane or *K − plane* was realized after its discovery in brass by Kirkendall and Smigelskas (Fig. 1(i)) [10], followed by theoretical developments by Matano and Darken [8,11]. Further experimental support was *inter alia* provided by inert molybdenum (Mo) wires acting as a marker plane (*K − plane*) between copper (Cu) and brass (Fig. 1(ii and iii)). This allowed quantification of shifts of the diffusion couple with respect to the marker plane. Although the Kirkendall effect appears straightforward, detailed research shows rather complicated processes taking place; such as, position splitting of the *K − plane*; the presence of multiple *K − planes* moving at different velocities and situations with stable versus unstable *K − planes* [5,6,12,13].

Here we report inter-diffusion studies of the Pt-Rh diffusion couple [3,12]. Furthermore, we aim to use this insight to *predict and tailor-make surface compositions of* $Pt_{100-x}Rh_x$ *bimetallic alloys prepared by deposition of Rh on single crystals of Pt, followed by thermal annealing; and in this way provide recipes on customized surface compositions of model systems for activity studies of heterogeneous catalysts.* Such model systems, with planar thin film geometry, will be prepared by e-beam evaporation of Rh onto the surface of polished Pt(100), Pt(110) and Pt(111) single crystals (SC), forming a polycrystalline Rh layer. We adopt methodologies that can be employed generically to develop custom compositions based bimetallic model systems; beyond the scope of the *multifoil* method [13]. Such optimization studies on PGM catalysts are crucial for certain processes, such as ammonia oxidation (Ostwald process) [14]. Firstly, we present experimental inter-diffusion results based on XPS and SEM/EDS analysis of Rh coated Pt single crystal surfaces. The data is then analysed in terms of two theoretical approaches; namely, the open planar thin film model for bi-metallic diffusion; and the more refined Darken analysis where we transition from ideal scenarios to descriptions that consider material properties. Finally, we suggest a more complex analysis where integrated diffusion coefficients are used. The theoretical basis of how to achieve greater accuracy in predicting concentration profiles as a function of depth, at surfaces, and deep within the bulk is presented.

2. Materials and methods

Sample Preparation: Pre-polished single crystals (SC) of platinum with (100), (110) and (111) orientations with one side polished to a roughness of $< 0.01\ \mu m$ and with an orientation accuracy of $< 0.1^{\circ}$ were sourced (MaTecK GmbH, purity 99.99 %) A Leybold L560 Electron − beam (e − beam) evaporation system was used to deposit rhodium films on to the polished surface of the Pt single crystals. Rh pellets (purity 99.99 %) were loaded in insulating crucibles and placed under high vacuum ($< 1 \times 10^{-6}\ mbar$). Test runs were carried out on Si-wafers for process calibration. Uniform layers of approximately 300 nm of Rh were deposited on *Pt − SC* surfaces at evaporation rates of *0.5 − 0.6 nm/min* at *40 − 60 W* power. After deposition, a sample was placed inside a quartz ampoule, evacuated and sealed. A Tesla Coil vacuum leak detector was used to confirm the quality of vacuum inside the ampoule. Ampoules were annealed at *1273 K* for periods of *3, 12* and *24 h*, respectively, before quickly being cooled in air. Subsequently, a Moorefield radio frequency (RF) sputtering system was used for deposition of a marker plane of crystalline zirconium dioxide ZrO_2 for SEM/EDS measurements on the Pt(100), Pt(110) and Pt(111) SC samples. Thickness and crystallinity control measurements were carried out for ZrO_2 depositions on SiO_2. The ZrO_2 films were directly deposited onto the pre-polished single crystals of platinum using an RF power of *100 W* with an argon gas flow (*12 sscm*), a substrate temperature of *~ 773 K* and a constant target-to-sample distance of *20 cm*. The pre-sputtering time was kept to half of the deposition time. Ellipsometry and profilometry were used to measure the thicknesses of the deposited materials. Grazing incidence angle X − ray diffraction (XRD) was used to confirm the crystalline nature of the films. *300 nm* of Rh was subsequently deposited and the samples were placed in evacuated ampoules and annealed, using the approach described above. Upon cooling the samples were cross-sectioned using a saw; mounted in conducting epoxy resin and polished. The SEM/EDS was used to characterize these samples.

Discs of polycrystalline platinum and a nominal *5 wt %* rhodium/platinum alloy were obtained from Birmingham Metal Company Ltd. The diameter and thickness of the discs were *5 mm* and *3 mm*, respectively. One side of each disc was polished to a *0.5 μm* finish, with successive grades of SiC and diamond abrasives. An interface marker consisting of a dispersion of corundum particles with a mean diameter of *1 μm* were deposited onto the polished surface of the Pt disc. The Pt disc was dried before contacting the *5 wt %* Rh/Pt disc. A load, consisting of a dense alumina cylinder with mass *400 g* was applied to the Pt − *5 wt %* Rh/Pt diffusion couple, which was then heated in an air muffle oven, to *1573 K*, for *200 h*. After annealing, the fused diffusion couple was mounted in resin,

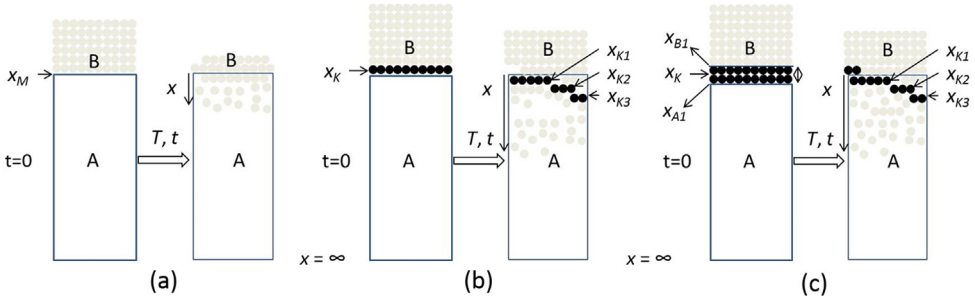

Fig. 1. Illustration of interdiffusion process in thin-film format taking place for metal A and metal B (a) without the use of an inert tracer; (b) by the use of a thin layer of tracer and (c) for an increasingly thicker tracer. x_K denotes the location of the tracer, *i.e.*, the K − plane, with x_{B1} and x_{A1} as additional planes forming due to the contact between metals A and B.

sectioned and polished. The inter-diffusion of platinum and rhodium was analysed using an Electron Beam Microprobe Analyzer (EMPA).

Measurements: Scanning electron microscopy (SEM) and energy dispersive spectroscopy (EDS) were performed using a Hitachi SU − 8200 CFE − SEM and a Bruker EDS system. For depth profiling, X-ray Photoelectron spectroscopy (XPS) and Argon plasma etching were used using a Kratos Axis Ultra DLD instrument. An achromatic Al-Kα source with an energy of *1486.6 eV* was used, with a chamber base pressure of ~ 1×10^{-9} *mbar*. Spectra were recorded for the BE range of *295–370 eV* and calibrated against the C1s peak carbon at BE of *284.7 eV*. After each sputtering cycle, XPS scans were recorded. The relative concentrations of Rh and Pt were obtained by evaluating the intensity of Pt $4f_{5/2}$ and Rh $3d_{5/2}$ doublets, after background subtraction. A flow diagram for the current sample preparation, analysis and simulation procedures are shown in Fig. A.1 (appendix). The etch rate (in *nm/min*) for the XPS depth profile crater was calculated using a sputter yield of ~ 5.2 Pt atoms per ion of Ar, material specific properties; including density (in kg/cm^3), molar weight (kg/mol) of Pt and ion current density (in A/m^2) [30].

EMPA analysis of the diffusion couple of the polycrystalline Pt − *5 wt %* Rh/Pt diffusion couple was carried out using a Cameca SX100 electron microprobe, equipped with five wavelength dispersive spectrometers. For analysis of the platinum and rhodium concentration profiles, a beam of *20 kV* and *20 nA*, with a count time of *30 s*, was used and Rh Lα (in differential mode) and Pt Lα (integral mode) emissions lines were scanned.

3. Theory

The thin film diffusion coefficient (TF − DC) was initially used to calculate the concentration profile as a function of time and depth. Subsequently, the TF − DC equation was adapted to describe tracer diffusion with respect to the substrate. The concentration gradient C_{TF} as a function of depth and time, at a given annealing temperature T, can be written as [4,5].

$$C_{TF}(x,t) = \frac{Q_{TF}}{\sqrt{\pi D_{TF} t}} exp\left(-\frac{x^2}{4D_{TF}t}\right) \quad (1)$$

where, Q_{TF} is the thickness of the deposited species (m); t is time (s); x is the distance (depth) in from the surface (m); D_{TF} is the diffusion coefficient (m^2/s) described by the classical Arrhenius equation $D_{TF} = D_0 \exp(-E_A/RT)$ with E_A as the activation energy (J/mol) and R the gas constant ($J/mol.K$), T the absolute temperature (K), and D_0 a pre-exponential factor (m^2/s). The slope of ln (C_{TF}) versus x gives the diffusivity of the species deposited. The calculation is frequently connected to solid-state diffusion studies by means of microprobe analysis and by taking interdiffusion into account; however, it is limited to systems where the total volume of the reacting species does not change after mixing. The initial contact plane, *i.e.*, the *Matano plane* (x_M) is located between the two reacting end members.

For the geometry shown in Fig. 1, we set the boundary conditions at t = 0, $A = A'$ for $x > 0$ and $B = B'$ for $x < 0$, where, A' and B' are the interface point or contact point for materials A and B. Boltzmann in his paper introduced the variable λ, related to time t, depth x and concentration in terms of $\lambda = \lambda(C_{TF}) = x/\sqrt{t}$, thereby relating concentration C_{TF} only to λ. This parabolic dependence of the composition in the diffusion zone as a function of time, lead Matano to formulate an equation for solid state interdiffusion [8].

$$D(C_{@x}) = -\frac{1}{2t}\left(\frac{dx}{dC}\right)_{C_{@x}} [A + B] \quad (2)$$

A limitation of this approach is the need to define the position of the Matano plane, x_M [25]. Furthermore, realistic diffusion situations typically leads to a change in total volume, which makes it difficult to accurately determine the initial contact plane (x_0). The Matano-Boltzmann relation provides average diffusivities and not diffusivities of the individual species.

Initial observations by Pfiel and Hartley gave impetus to Smigelkas and Kirkendall to examine inequalities in diffusivities of Cu-Zn with Mo placed as an inert marker. This subsequently became known as the Kirkendall effect [9,10,22,26]. These experiments showed that Zn diffused faster than Cu resulting in the movement of the inert marker, and that the migration of Zn resulted in vacancies that later became occupied by Cu, or, if the system was not given ample time to relax plastically, formation of voids that consisted of coalesced vacancies. Later, Darken as well as Hartley and Crank separately treated solid state diffusion mathematically by considering multiple DCs [11,23].

Let us consider a binary system with metallic species A and B with an inert marker (K − plane) at the A-B interface. Furthermore, let the intrinsic diffusivity of species B (D_B) be greater than of species A (D_A), which means that the *K − plane* will move towards species A. We assume that the interdiffusion does not change the total volume upon mixing. V_m is the total molar volume, V_A is the partial molar volume of species A and V_B is the partial molar volume of species B. D_{tot} *is given by:*

$$D_{tot} = V_A C_A D_B + V_B C_B D_A \quad (3)$$

and for $V_m = V_A = V_B$, where partial molar volume remains constant and equal, such as in the ideal scenario, we get the simplified Darken equation,

$$D_{tot} = N_A D_B + N_B D_A \quad (4)$$

where N_A and N_B are the mole fractions of species A and B, respectively. In a non − ideal scenario, the total volume would tend to change upon mixing. Hence, the Boltzmann approach is followed, denoting $x = x - x_0$ (with $x_0 = 0$) as the distance from the initial contact plane at x_0 with a parabolic dependence of total volume with respect to time of diffusion.

For a non − ideal system [24], with μ_A and μ_B as the chemical potentials of materials A and B and mobility $m_i = \nu_i/F$ where F is the force exerted due to chemical potential and ν_i is the velocity of species (i = A or B), we obtain,

$$D_i = m_i C_i \frac{d\mu_i}{dC_i} \; and \; J_i = -D_i \frac{dC_i}{dx} \quad (5)$$

The potential μ_i is given as $\mu_i^0(T,P) + RTlna_i$, J_i is the flux of species, and D_i is the diffusion coefficient of species i; a_i is the activity $a_i = \gamma_i N_i$ where γ_i is the activity coefficient, and R is the gas constant. Finally, the chemical potential of species i is,

$$\mu_i^0(T,P) + RT(lnN_i + ln\gamma_i)$$

The diffusion coefficient can then be written as,

$$D_{B/A} = \frac{V_m}{V_{A/B}} m_B RT\left(1 + \frac{dln\gamma_{B/A}}{dlnN_{B/A}}\right) \quad (6)$$

or

$$D_{B/A} = D^{@x}_{B/A}\frac{V_m}{V_{A/B}}\frac{dlna_{B/A}}{dlnN_{B/A}} = D^{@x}_{B/A}\frac{V_m}{V_{A/B}}\left(1+\frac{dln\gamma_{B/A}}{dlnN_{B/A}}\right)$$

where $D_i^{@x} = m_i^{@x}RT$ is the Nerst-Einstein relation.

By means of the Gibbs-Duhem relation, we relate the thermodynamic factor as, $\Phi = \frac{dlna_A}{dlnN_A} = \frac{dlna_B}{dlnN_B}$, and describe the diffusion of B into A and vice versa by the modified Darken equation [11].

$$D_{tot} = \left(N_A D_B^{@x} + N_B D_A^{@x}\right)\left(\frac{dlna_B}{dlnN_B}\right) \quad (7)$$

By integrating the total DC as a function of mole fraction of species (N_i) with limits being the values at the plane of contact of species A and B with the tracer, and by representing the energy per mole of disassociation at the two interfaces, we can rewrite the total diffusion coefficient given by Darken as [25].

$$D_{tot} = -\left(N_A D_B^{@x} + N_B D_A^{@x}\right)\frac{N_i\Delta_f G_B^0}{RT} \quad (8)$$

where, $\Delta_r G_B^0$ is the Gibbs energy of net reaction per mole of species B moving from interface *B1* to *A1* (see Fig. 1), given by $\Delta_f G_\beta^0 = (1-\boldsymbol{x})\Delta_r G_{Rh}^0 = \boldsymbol{x}\Delta_r G_{Pt}^0$ and $\Delta_r G^0 = -RT(lna^{II} - lna^{I})$. Therefore, *lna* can be described as the activity of the two metals A and B which is directly related to the temperature, gas constant and chemical potential of the two respective metals and is given by the relations.

$\mu_{A/B} = \mu^0_{A/B} + RT\ ln\ a^{I/II}_{A/B}$ where, $ln\ a^{I/II}_{A/B} = \gamma_{A/B}N_{A/B}$

Finally, the Kirkendall marker velocity is expressed as,

$$v_K = \frac{1}{V_m}\left(V_B D_B^{@x} - V_A D_A^{@x}\right)\Phi\frac{\partial N_i}{\partial x} \quad (9)$$

Interdiffusion, where we consider critical material properties and which takes into account the integrated diffusion coefficient is to the authors' understanding, the most realistic theoretical approximation. However, further analysis with this approach is beyond the scope of this paper.

4. Results and discussion

4.1. Interdiffusion data based on XPS and SEM/EDS analysis on rhodium coated platinum single crystal surfaces

The Pt(110) – SC represents a crystallographic orientation where the structure is neither as open as (100), nor as closed packed as (111). *300 nm* of rhodium was deposited on a Pt(110) – SC, annealed and finally analysed by XPS depth profiling. Fig. 2(a) shows the Rh – gradient *versus* depth (x) extracted from the intensity of the XPS Rh $3d_{5/2}$ doublet at a binding energy (BE) of *306.5* eV; which is characteristic of metallic Rh [29]. Although the initial (surface) Rh – concentration after *12 h* annealing drops to around half of the concentration observed after *3 h* annealing, the final depth for dispersion of Rh into the Pt(110) – SC is only marginally affected by the prolonged *12 h* annealing. These observations address key questions concerning the Rh permeation. Is Rh diffusing at a higher rate in the *ab* – plane compared to the orthogonal direction; and is movement of Rh from the deposited films into Pt limited by a vacancy mechanism in the perpendicular direction, or vice versa? Indicative answers based on SEM/EDS results are shown for all three Pt crystal orientations in Fig. 2(b). These show varying depths of Rh – penetration dependent on crystal orientation. Additional processing and characterization was carried out for samples annealed for *24 h*, including EDS measurements of cross sections, with a ZrO_2 inert marker (Fig. 2(b)). This gave consistent quantitative results.

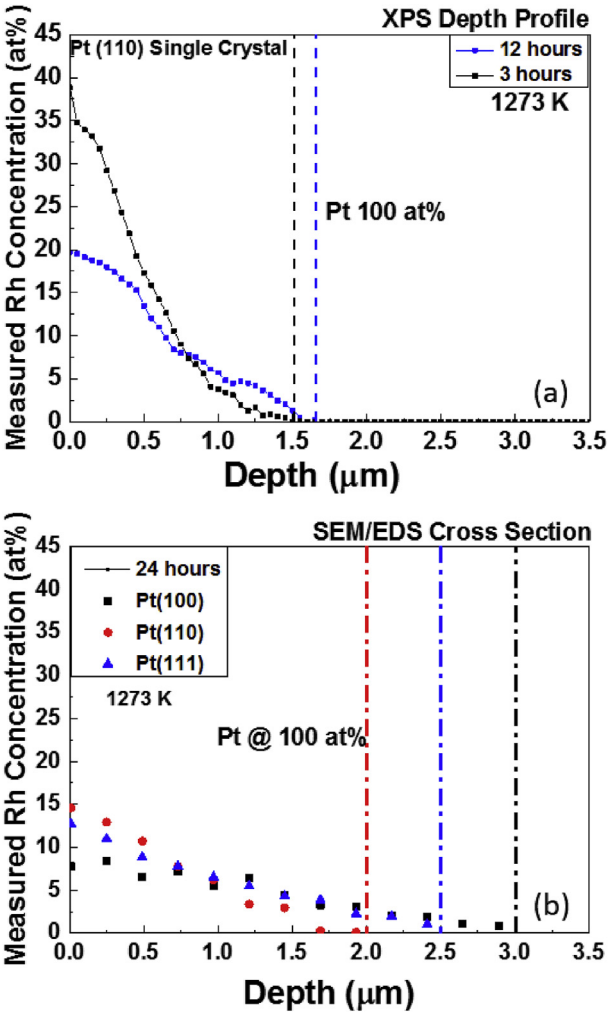

Fig. 2. Concentration profiles for *300 nm* thick Rh depositions of Pt followed by *3*, *12* or *24 h* annealing at *1273 K*; (a) XPS depth profile measurements on Pt(110), and (b) SEM/EDS cross section data for all three orientations of the Pt single crystals.

Qualitative SEM micrographs of Pt(110) surfaces are shown in Fig. 3 for three cases; *as – deposited*, and after vacuum anneals of *3* and *24 h*. We note that Rh is present as either a smooth and uniform film following the contours of the polishing scratches, or as small particles with sizes from a few tens of nm up to a few hundreds of nm; as a result of the directional deposition in the e-beam evaporator. The former reflects a fully alloyed Pt – Rh bimetallic solid solution, while the latter grains are probably just partially alloyed. Qualitative and quantitative results show that inter-diffusion during *3* and *24 h* anneals at *1273 K* reduces the Rh surface concentration from *40 at %* (*3 h*; Fig. 3(b)) to around *10 at %* after *24 h* (Fig. 3(c)). At the same time, the surface becomes less corrugated. Detailed inspection shows that the *24 h* anneal gives rise to segregated sections/areas; *i.e.*, smooth areas of fully alloyed Pt – Rh areas and rough sections of partially or incompletely alloyed Pt – Rh (see Fig. 3(c)). Furthermore, EDS indicates enhanced Rh concentrations in the rougher sections. The EDS analysis shows that the average Pt – Rh concentration at the surface depends on the crystal orientation; *i.e.*, *Pt(100) – Rh: 7.8 at %*; *Pt(110) – Rh: 14.7 at %* and *Pt(111) – Rh: 12.7 at %* Rh. The Pt(110) SC surface shows the

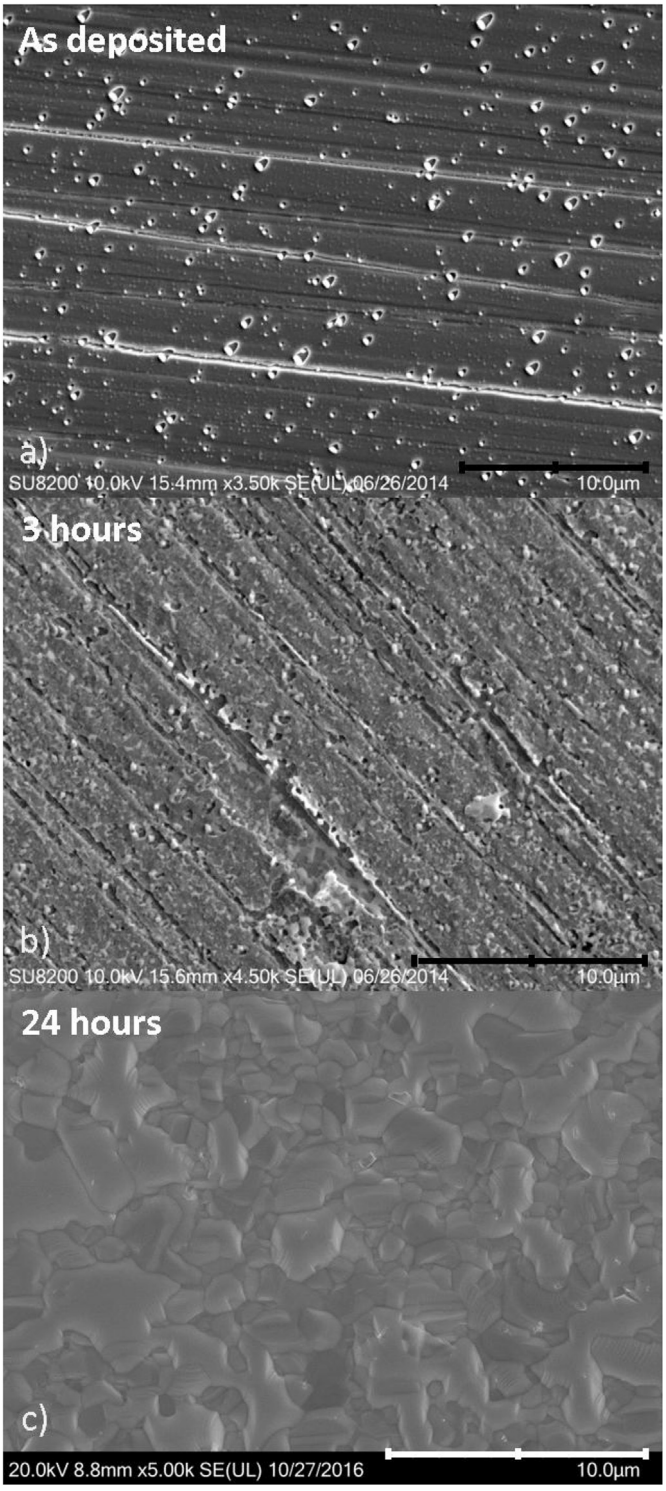

Fig. 3. SEM images of surface (a) of Pt(110) single crystal coated with *300 nm* layer of Rh showing smooth depositions following the surface polishing scratches with numerous pits and embedded metal particles scattered over the surface: (b) alloying process at *1273 K* after *3 h* annealing showing initiation of Rh – Rh and Pt – Rh alloying process at interfaces of polishing scratches and radiating outwards. Metal particles reside inside pits; (c) after annealing at *1273 K* for *24 h*, showing the surface segregation into two sections: one, with fully alloyed Pt – Rh smooth layers, other with partially alloyed Pt – Rh rougher sections.

highest concentration of Rh, and hence the lowest inwards diffusivity. Intuitively, one would have expected the lowest interdiffusion rate for the close packed Pt(111) SC orientation. For Pt(110) the SEM analysis shows, after annealing for *24 h* at *1273 K*, a large amount of surface Rh, and the original polishing marks are not visible. For the corresponding annealed Pt(100) and Pt(111) surfaces, the scratch marks are still clearly visible, see Fig. 4 and Fig. A.2 (appendix).

For all of these orientations, we note that the scratch marks act as initiators of the alloying process that distributes outwards (Fig. 4

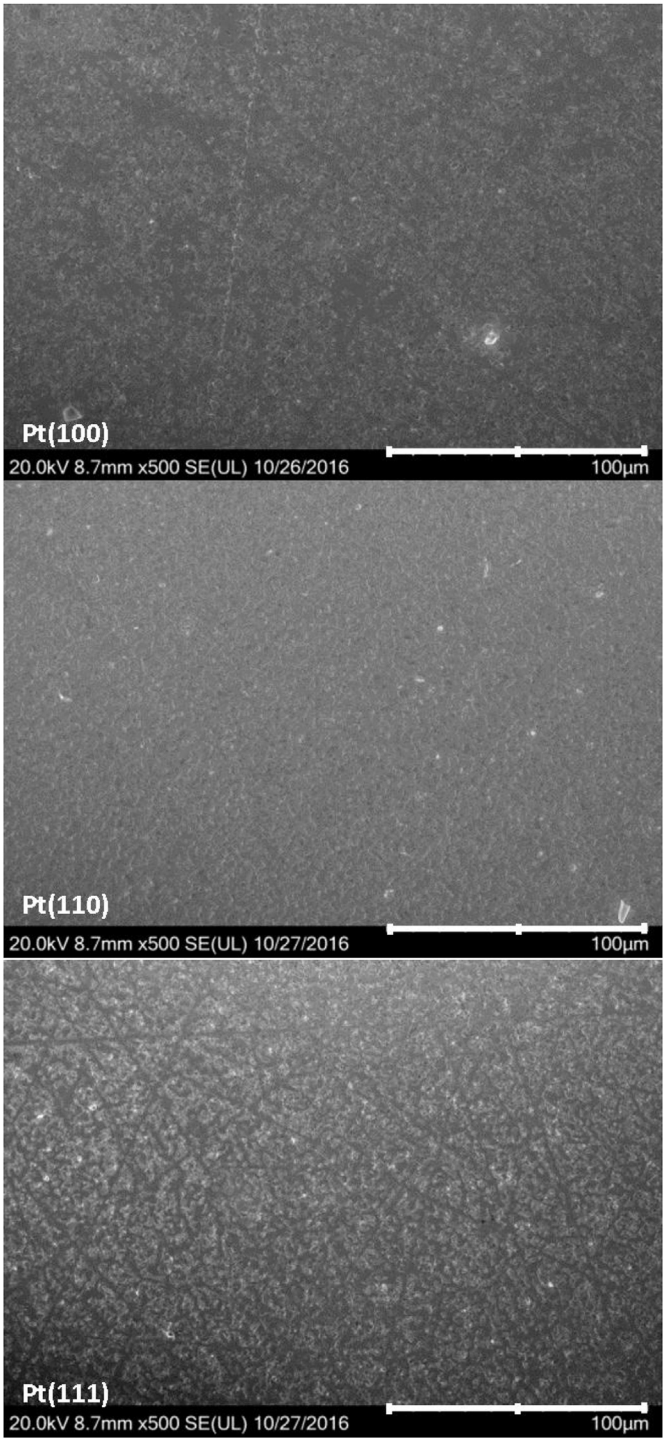

Fig. 4. SEM wide scans of Pt single crystal surfaces after deposition of *300 nm* Rh and annealing of *24 h* at *1273 K*. Notice the apparent lack of polishing scratches for Pt(110) suggesting less diffusion of Rh into Pt(110) than for Pt(100) and Pt(111).

and A.2 (appendix)). The extent of alloying differs between the crystal orientations; Pt(100) exhibits the highest degree of alloying, whereas Pt(110) exhibits the least, suggesting a complex inter-diffusion process. XRD measurements (not shown) carried out on all 3 Pt single crystals with Rh on the surface and after *24 h* annealing, indicate that all 3 single crystals were grown in identical conditions and vary only in their cut orientation. Furthermore, the crystallites of Pt in all three samples are of similar size of $100 \pm 10\,nm$, whereas, for Rh indications point to presence of nanocrystallites of $\leq 10\,nm$ sizes.

The alloyed crystals were cross-sectioned using a diamond saw and embedded in a copper loaded epoxy. The SEM micrographs, labelled $\boldsymbol{a} - \boldsymbol{d}$ in Fig. 5 (and in supplementary Figs. A.2 and A.3 (appendix)), along with corresponding EDS maps, show localization of Rh within the top few microns from the sample surface, and not deeper into the bulk. The use of a ZrO_2 $K-plane$ marker in these experiments permitted gathering of quantitative information from the SEM/EDS data, see Fig. 5, A.2 and A.3 (appendix).

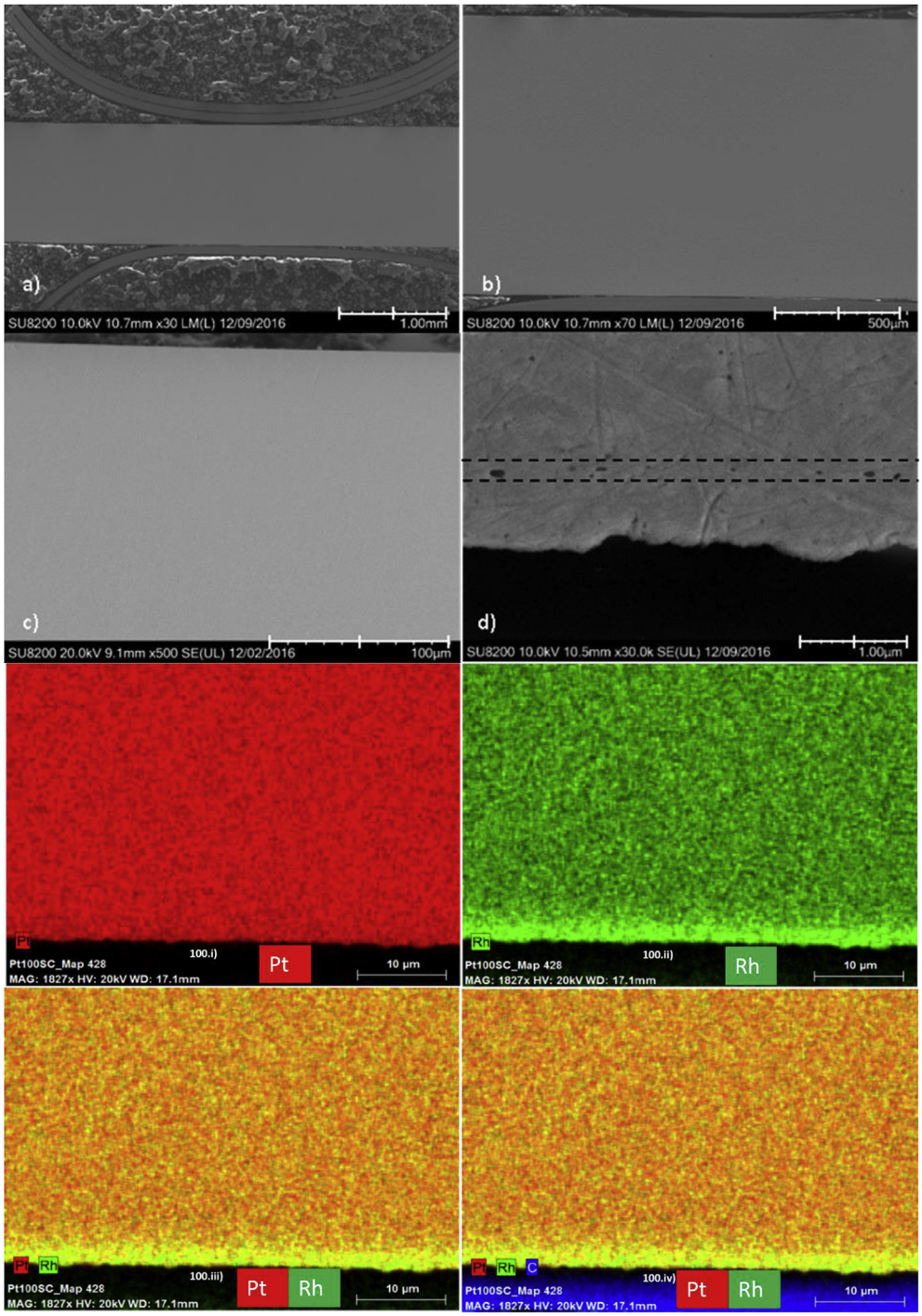

Fig. 5. (top) SEM micrographs of Pt(100) (a–d) coated with *300 nm* of Rh and alloyed at *1273 K* for *24 h*, see scale bar $1 - 500\ \mu m$. Notice the voids due to unstable K – plane formation; and (bottom) EDS cross section maps of Pt, Rh, Pt + Rh for Pt(100), scale bar *10 µm*, clearly showing the depth based decay of Rh concentration (Pt in red, Rh in green). (For interpretation of the references to colour in this figure legend, the reader is referred to the Web version of this article.)

Following the *multifoil* method, a *15 nm* thick crystalline ZrO_2 film was included by sputtering [12,18]. It was not possible to locate this ZrO_2 marker by direct observations of the deposited oxide layer; however, the presence of voids and plate-like inclusions nevertheless clearly identified the stable $K-plane$ for the Pt − Rh couple. The $K-plane$ velocities were obtained for the three crystal orientations; $v = x/2t$ where v is velocity of $K-plane$ on diffusion, x is depth at which the plane is observed and t annealing time, see Table A.1 (appendix). Based on knowledge of depth, temperature and time, experimental diffusion coefficients (DC) were extracted from SEM/EDS, and as well as from XPS depth profiling measurements.

Fig. 5 visualizes the Pt and Rh distributions in red and green, respectively. The elemental maps are overlaid in Fig. 5, A.2 and A.3 (appendix). In the SEM micrographs, voids and plate-like inclusions are visible. These are attributed to a single stable $K-plane$ that forms inside a diffusion zone when the gradient of the velocity is *negative* at the intersection point [13]. These voids or plate-like inclusions are present for all studied SC orientations, but most clearly seen for Pt(100). The EDS mapping shows that Rh is concentrated towards the surface and is not present in measurable quantities in the bulk below a certain limiting depth '*x*' of a few microns. This is evident from Fig. 5, A.2 and A.3 (appendix) where relevant EDS cross section maps for the various orientations are labelled as ***(100i-iv)***, ***(110i-iv)***, and ***(111i-iv)*** respectively. These observations confirm that the inter-diffusion depends on crystal orientation (Table 1).

4.2. Diffusion coefficients (DCs), activation energies and Kirkendall (K) plane velocities

The current work represents to our knowledge, the first study of the Pt − Rh diffusion couple in a vacuum environment with heat as the sole promoter of diffusion. In earlier studies, using XPS and Atom Probe Tomography (APT) [2,20,21] for characterization, both atmosphere and temperature acted as promoters.

The anneal temperature of *1273 K* is highly relevant for Pt − Rh catalysts in the Ostwald and Andrussow processes. For our analysis, we first take note of Li et al. [1] who used Fick's first law to calculate the $D_{Rh\rightarrow Pt}$ DCs at *873*, *973* and *1073 K*, albeit in oxidative environment. Furthermore, we adopt self-diffusion values of Pt into Pt, $D_{Pt\rightarrow Pt}$ as tabulated in the Smithells Metals Reference Book [15]. Based on their APT studies, Li et al. reported an activation energy of $E_a = 2.63\ eV$. Our single crystal studies gave however a somewhat higher activation energy at *1273 K*, see below.

Based on quantitative XPS depth profiling the progress of the alloying reaction for a Pt(110) single crystal coated with 300 nm of Rh was followed. As seen in Fig. 2(a), the surface Rh concentration after annealing at *1273 K* is reduced from *40 (3 h* annealing*)* to *20 at % (12 h)*. The measured DC of Rh into Pt(110) is then $D_{measured}$ $(3\ h,\ 1273\ K) = 8.68\times10^{-17}\ m^2/s$ and $D_{measured}$ $(12\ h,\ 1273\ K) = 2.46\times10^{-17}\ m^2/s$ (Table A.1 (appendix)) using the simple expression $x = 2.4\sqrt{Dt}$, where x is depth, D is the diffusion coefficient and t time. Note, the extent of interdiffusion could at this stage not be settled, since, a $K-plane$ is needed to determine the relative velocities of Pt and Rh the Pt-Rh diffusion couple. For this reason, ZrO_2 was introduced as a $K-plane$. This modified approach gave data on the kinetics and DCs, on $K-plane$ velocity, and surface/bulk compositions of the Pt − Rh model catalysts (Table 1 and A.1 (appendix)).

Pt − SCs, with (100), (110) and (111) orientations; , all with a $K-plane$ inserted to follow the interdiffusion gradient, were annealed for *24 h at 1273 K*, cross-sectioned and analysed by SEM/EDS. For diffusivity evaluations, multiple data points were collected for the three samples (see Fig. 2(b)) as a function of depth by means of SEM/EDS analysis. Two aspects stand out immediately. First, the depth of alloying marginally changes as anneal time is doubled from *12* to *24 h*. Second, we observe a variation in rate of interdiffusion which is dependent on crystal orientation. This is in line with earlier reports. In 1986, Preuss et al. described a directional dependence for surface self-diffusion due to anisotropic surface energy, with preference for $[1\bar{1}0]$ compared to [001]. They further reported an activation energy of *1.7 eV* for $[1\bar{1}0]$ and *3.2 eV* for [001] based on measurements by the periodic profile decay technique, at *1650 K* [16]. Field ion microscopy (FIM) and scanning tunnelling microscopy (STM) studies on so-called one-dimensional surfaces, e.g. Pt(110), and two-dimensional surfaces, e.g. Pt(100) and Pt(111), indicate substantial variations in activation energies for ad-atom movements (nearest neighbour or jumping) and with respect to bulk (atom exchange) diffusion [17]. The current observation that the depth of alloying does not change with increasing annealing time, may possibly be associated with the different lattice constants (a_0) for the two elements [27]. Platinum has a larger lattice constant $a_0 = 3.924\ Å$ than rhodium; $a_0 = 3.803\ Å$. This might suggest that the crystal structure of Pt would be more accommodating towards Rh atoms in a vacancy driven interdiffusion process, in comparison to Rh accommodating larger Pt atoms.

The SEM/EDS data was used to extract diffusion coefficients of Rh into Pt − SC similar to the XPS scenario described above. The results are $D^{Rh\rightarrow Pt(100)}_{measured}$ $(24\ h,\ 1273\ K) = 1.8\times10^{-17}\ m^2/s$, $D^{Rh\rightarrow Pt(110)}_{measured}$ $(24\ h,\ 1273\ K) = 8.0\times10^{-18}\ m^2/s$ and $D^{Rh\rightarrow Pt(111)}_{measured}$ $(24\ h,\ 1273\ K) = 1.2\times10^{-17}\ m^2/s$, respectively. By utilizing the pre-exponential diffusion factor for Pt self-diffusion $D_0 = 2.2\times10^{-5}\ m^2/s$ [15] and the measured diffusion coefficient for Rh into Pt, we extract an activation energy for our system of ~3.15 eV using the Arrhenius equation, $D = D_0\exp(-E_A/kT)$ at *1273 K*. We furthermore extracted experimental DC for Pt diffusing into Rh, and found all three Pt-orientations to be very close to $D^{Pt(100,\ 110,\ 111)\rightarrow Rh}_{measured}$ $(24\ h,\ 1273\ K) \approx 1.6\times10^{-19}\ m^2/s$. The activation energy determined by us is higher than the literature value, see above, but refers notably to a sample annealed in vacuum at temperatures representative for the calculated DC. Using a separate approach, we derived the diffusion coefficient of $5.8\times10^{-14}\ m^2/s$ at *1573 K* (see Table A.2 (appendix) and experimental).

Calculated DCs are shown in Fig. 6 and in Table A.2 (appendix). By using the current activation energy of ~ *3.15 eV* at *1273 K* in a modified Arrhenius equation, a jump rate of $w = 1.1\ s^{-1}$ is calculated according to $w = \nu_0\exp(-E_A/kT)$, and with a calculated vibrational frequency for Rh into Pt of $\nu_0 = 3.0\times10^{12}\ s^{-1}$. Conversely, for Pt into Rh, the calculated vibration frequency is $2.3\times10^{12}\ s^{-1}$ which gives a jump rate of $w = 0.8\ s^{-1}$. Taking into account the cubic (ccp/fcc) structure for Pt and that the diffusion takes place by a vacancy mechanism, the 3 − D total jump frequency, Γ is calculated to be $6.3\ s^{-1}$ for Rh into Pt and $4.7\ s^{-1}$for Pt into Rh. Hence, in a 3 − D metal structure, 6.3 diffusional jumps take place *per second* for Rh into Pt and 4.7 diffusional jumps take place *per second* for Pt into Rh, resulting in propagation of the $K-plane$ towards the Pt-SC. The DC of vacancies in both the Pt and Rh systems is $\sim10^{-19}\ m^2/s$, and comparable to the Pt into Rh DC values.

Table 1
Measured diffusion coefficient (DC) for Rh into Pt and Pt into Rh for three crystal orientations from SEM/EDS data (*24 h* anneal at *1273 K*).

SEM/EDS	Pt(100)	Pt(110)	Pt(111)
Rh into Pt (m^2/s)	3.0×10^{-17}	8.0×10^{-18}	1.2×10^{-17}
Pt into Rh (m^2/s)	1.6×10^{-19}	1.5×10^{-19}	1.6×10^{-19}

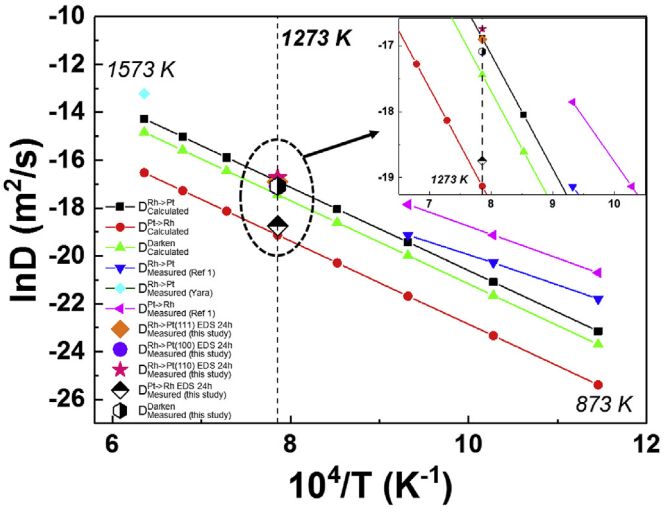

Fig. 6. Calculated and measured diffusion coefficients (DCs). Black points show the calculated DC of Pt into Rh, whereas calculated values for Rh into Pt are marked in red. Blue and magenta show reported values by Li et al., whereas cyan shows a measured DC at Yara International. Points marked as orange diamond (solid), violet circle (solid), and pink star (solid) show experimental DC of Rh into Pt(111), Pt(100) and Pt(110) derived from SEM/EDS data. Finally, black diamond (half-solid) and black hexagon (half-solid) show measured DC and measured Darken DC of Pt into Rh. Same data in blown up is shown in inset [1,15].[1,15]. (For interpretation of the references to colour in this figure legend, the reader is referred to the Web version of this article.)

Diffusion kinetics for the $K-planes$ (K_{100}, K_{110} and K_{111}) were indirectly derived from observations of the movement of the ZrO_2 inert markers by SEM/EDS, see Fig. 7 (c) and Table A.1 (appendix). The velocities of Rh and Pt inter-diffusion are relatively similar and in the range of $1.4 \times 10^{-12}\ m^2/s$ for Pt(110), $1.7 \times 10^{-12}\ m^2/s$ for Pt(111) to $2.6 \times 10^{-12}\ m^2/s$ for Pt(100). It is seen that Pt(110) has the slowest moving $K-plane$ which shifts by just $250\ nm$ from its initial position of $x_0 = 300\ nm$ on the x-axis in Fig. 7 to $x_K = 550\ nm$ after $24\ h$ annealing at $1273\ K$. The $K-plane$ moves towards the Pt − SC and K_{110} is given as $x_K - x_0$, *i.e.*, $550 - 300\ nm = 250\ nm$. Similarly, for Pt(111) the $K-plane$ is moved $300\ nm$ towards Pt − SC whereas the shift is $450\ nm$ for Pt(100). The observed concentration profiles for all crystal orientations, and the fact that the $K-planes$ cross in a negative gradient, shows that the formed planes are stable in the inter-diffusion zone, consistent with formation of voids and plate-like inclusions. This is similar to what reported for the Au − Zn system [13]. We note that $K-planes$ are shifting towards the Pt − SC for all crystal orientations. Therefore, we expect that extended annealing beyond $24\ h$ will lead to steady Pt enrichment of the surface. Likewise, an assimilation of Rh into the Pt − SC will occur, thereby creating a more complex concentration gradient in the alloy. The observed differences in movement of the $K-plane$ with respect to crystal orientation is consistent with different bulk diffusivities for the current model materials at microscopic and macroscopic scales.

The concentration $C(x,t)$ of *Rh vs. Pt* was calculated according to different approximations based on our experimentally determined

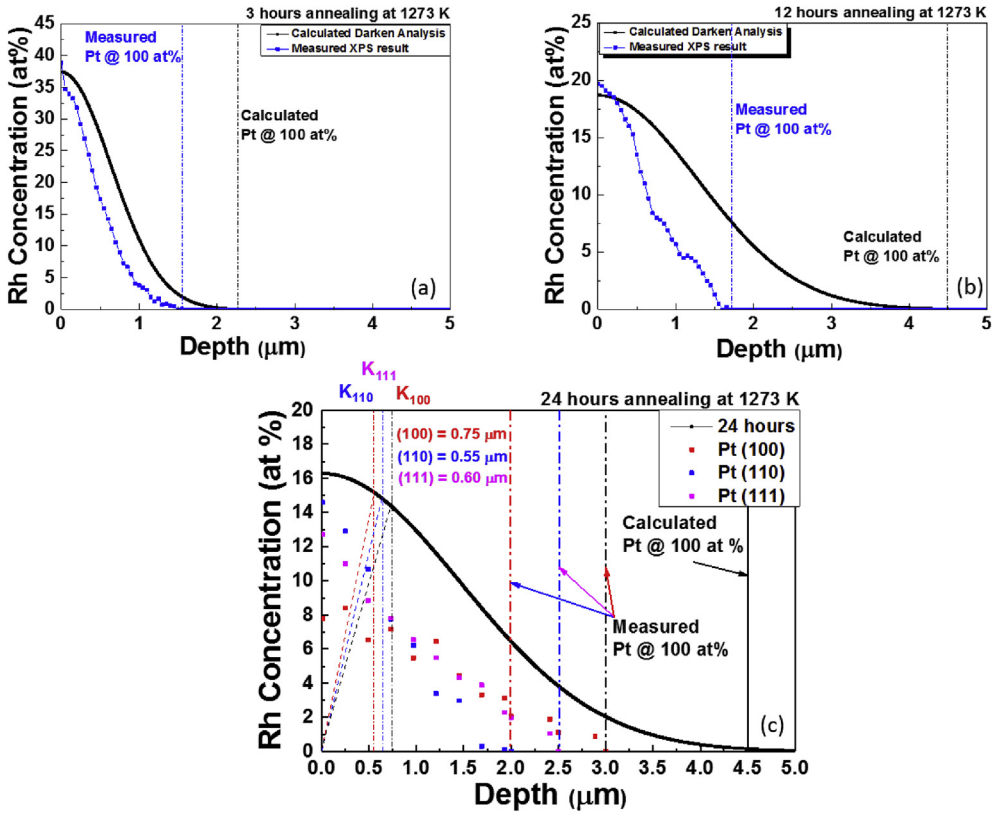

Fig. 7. Comparison between calculated (black line-symbol) and measured Pt − Rh concentration profiles. The calculated concentrations profiles are derived using an activation energy of $3.15\ eV$ at temperature of $1273\ K$ using diffusion coefficients from the Darken equation (4) and introduced into equation (1). The calculated curves signify ideal concentration variations keeping in mind the limiting conditions; (a, b) measured concentration of rhodium (blue) for 3 and $12\ h$ annealing at $1273\ K$, respectively, for a system with $300\ nm$ deposited Rh on Pt(110) and analysed by XPS; (c) measured concentration of rhodium after annealing for $24\ h$ for $300\ nm$ of Rh deposited on Pt(100) (red points), on Pt(110) (blue points) and Pt(111) (magenta points) as derived by SEM/EDS cross section analysis. Vertical dotted lines show depths where Rh concentration has dropped to zero within measurement uncertainty. The positions of the Kirkendall markers (apparent as voids in SEM cross sections), *i.e.*, K − planes, are shown for the three Pt − SC orientations (K_{100}, K_{110}, K_{111}). (For interpretation of the references to colour in this figure legend, the reader is referred to the Web version of this article.)

DC at *1273 K; (for details see Theory section)*. Thin − film diffusion values were calculated according to Equation (1) keeping in mind diffusion of Rh into Pt and vice versa. For results see Fig. 5 and Table A.1 (appendix). Secondly, the Darken equation (equation (4)) was used to calculate DC in the absence of a $K-plane$ inert tracer. These theoretically calculated concentration profiles (Fig. 7(a) and b) obtained from equation (1), where D was derived either using standard Ficks's law or equation (4) and were compared with XPS measured profiles. Although, there is very good agreement with respect to the initial Rh concentration and the concentration slope for *3* and *12 h* annealing, there are significant discrepancies for depths beyond $2-3\,\mu m$. One likely reason is that these models neglect material properties such as the effect of changing Rh to Pt content (chemical potential) during the progressive inter − diffusion.

The diffusion parameters obtained from SEM/EDS measurements are shown in Table A.1 (appendix) and are seen to be in good, to very good agreement with the calculated DCs according to Equation (4), *i.e.*, the Darken equation and an activation energy of $E_a = 3.15\,eV$ (see Table A.2 (appendix)). However, the discrepancy between calculated and measured concentration profiles for the XPS data (Equation (4), $E_a = 3.15\,eV$) remains; also for the SEM/EDS data, Fig. 7(c). The data shows a good to very good agreement between the surface concentrations of Rh on Pt(110) and Pt(111), but, not for Pt(100), where the observed surface concentration is far less than calculated. Concomitantly, the observed penetration depth for Rh diffusion (*i.e.*, 100 at% Pt level) is largest for Pt(100); $\sim 3\,\mu m$ compared with $\sim 2.0\,\mu m$ for Pt(110) and $\sim 2.5\,\mu m$ for Pt(111). The discrepancy to the calculated depth is smallest for Pt(100), see Fig. 7(c). We conclude that the current methodology may predict concentration profiles of PGM alloys down to a depth of up to $2-3\,\mu m$.

Fig. 6 highlights the experimental (measured) results overlaid with theoretical (calculated) values from Table A.2 (appendix) using Equation (1) with D derived from Fick's law and equation (4) (Darken equation). The measured DC values by Li et al. had an oxygen environment as additional promoter apart from heat, and gave a higher value for Pt diffusion into Rh. Both platinum and rhodium form volatile oxide species which affect the metal diffusion towards the oxygen atmosphere [1,19,28]. We note an excellent match between our measured and calculated diffusion coefficients with respect to both Rh into Pt as well as Pt into Rh inter-diffusion. As far as the authors are aware, it is for the first time a purely measured value of Pt into Rh DC has been obtained.

5. Conclusion

The current approach provides good agreement between simulated and observed surface compositions of the Pt single crystals after Rh deposition and high temperature annealing. This verification is essential for future tailoring of the surface composition of PGM crystals for studies of catalytic activity towards processes of industrial importance such as the Oswald- and the Andrussow processes. In this work, we successfully developed an experimental methodology utilizing XPS depth profiling and SEM/EDS cross section analysis for determination of concentration profiles due to interdiffusion of metal A into metal B in bimetallic PGMs. For the first time experimental DC of Pt into Rh in an environment with temperature as the sole promotor is extracted. We observed that the DC values depends on the crystallographic orientation of the Pt − SC. Platinum single crystals of orientation (110) display the lowest $K-plane$ velocity and extracted DC, whereas crystals with an (111) orientation show an intermediate behaviour. In the case of (100) orientated crystal, a far larger movement of Pt − Rh species takes place with DCs coming closer to the calculated values from Darken analysis. Theoretical calculations may be used for screening and comparison with experimental values for an extended number of PGM alloys. In this way, the methodology may become an important tool for achieving desired surface compositions in PGM model catalysts.

Acknowledgements

The project has received financial support from the Research Council of Norway via the TOPCAT project (GASSMAX, Grant number 215461/E30) and the industrial Catalysis Science and Innovation Centre (iCSI) (Grant number 237922). The authors would like to thank Dr. Yang Hu at FASE and Vegard Skiftestad Olsen at the LENS group at the University of Oslo for their support.

Appendix A. Supplementary data

Supplementary data to this article can be found online at https://doi.org/10.1016/j.jallcom.2019.02.026.

References

[1] T. Li, E.A. Marquis, P.A.J. Bagot, S.C. Tsang, G.D.W. Smith, Catal. Today 175 (1) (2011) 552–557.
[2] T. Li, P.A.J. Bagot, E.A. Marquis, S.C.E. Tsang, G.D.W. Smith, J. Phys. Chem. C 116 (33) (2012) 17633–17640.
[3] M. Kalyva, D.S. Wragg, H. Fjellvåg, A.O. Sjåstad, ChemistryOpen 6 (2) (2017) 273–281.
[4] A. Fick, Ann. Phys. 170 (1) (1855) 59–86.
[5] J. Crank, The Mathematics of Diffusion, Oxford university press, 1979.
[6] G.v. Hevesy, W. Seith, Z. Elektrochem. 37 (1931) 528–531.
[7] G. Grube, u.A. Jedele, Z. Elektrochem. angew. phys. Chem. 38 (10) (1932) 799–807.
[8] C. Matano, Jpn. J. Phys. 8 (1933) 109–113.
[9] L. Pfeil, J. Iron Steel Inst., London 119 (1929) 501–547.
[10] A. Smigelskas, E. Kirkendall, Trans. Aime 171 (1947) (1947) 130–142.
[11] L.S. Darken, Trans. Aime 175 (1948) 184–201.
[12] T. Heumann, G. Walther, Z. Metall. 48 (4) (1957) 151–157.
[13] M. Van Dal, A. Gusak, C. Cserháti, A.A. Kodentsov, F. Van Loo, Phys. Rev. Lett. 86 (15) (2001) 3352.
[14] L.B. Hunt, Platin. Met. Rev. 2 (4) (1958) 129–134.
[15] W.F. Gale, T.C. Totemeier (Eds.), Smithells Metals Reference Book, eighth ed., Butterworth-Heinemann, Oxford, 2004, 13-1-13-120.
[16] E. Preuss, N. Freyer, H. Bonzel, Appl. Phys. A 41 (2) (1986) 137–143.
[17] G. Antczak, G. Ehrlich, Cambridge University Press 2010.
[18] M. Van Dal, M. Pleumeekers, A.A. Kodentsov, F. Van Loo, Acta Mater. 48 (2) (2000) 385–396.
[19] J. Merker, D. Lupton, M. Töpfer, H. Knake, Platin. Met. Rev. 45 (2) (2001) 74–82.
[20] T. Wang, L. Schmidt, J. Catal. 71 (2) (1981) 411–422.
[21] T. Li, P. Bagot, E. Marquis, S.E. Tsang, G.D.W. Smith, Ultramicroscopy 132 (2013) 205–211.
[22] G. Hartley, Trans. Faraday Soc. 42 (1946) B006–B011.
[23] G. Hartley, J. Crank, Trans. Faraday Soc. 45 (1949) 801–818.
[24] C. Wagner, Acta Metall. 17 (2) (1969) 99–107.
[25] A. Paul, Laboratory of Materials and Interface Chemistry, 2004.
[26] L. Darken, R. Gurry, Physical Chemistry of Metals, McGrawhill, New York, 1953.
[27] R. Scheidecker, M. Berard, J. Am. Ceram. Soc. 56 (4) (1973) 204–206.
[28] T. Werber, Z. Zurek, A. Jaron, ECS Trans. 16 (44) (2009) 109–121.
[29] A. Munoz, G. Munuera, P. Malet, A.R. Gonzalez-Elipe, J.P. Espinos, Surf. Interface Anal. 12 (1988) 247–252.
[30] http://www.npl.co.uk/science-technology/surface-and-nanoanalysis/services/sputter-yield-values (Last accessed: August, 2018).